

Resonant tunneling as a dominant transport mechanism in n -GaAs/ p -GaAs tunnel diodes

K. Jandieri,^{1,a)} S. D. Baranovskii,¹ O. Rubel,¹ W. Stolz,¹ F. Gebhard,¹ W. Guter,² M. Hermle,² and A. W. Bett²

¹Department of Physics and Material Sciences Center, Philipps University Marburg, D-35032 Marburg, Germany

²Fraunhofer Institute for Solar Energy Systems, Heidenhofstr. 2, D-79110 Freiburg, Germany

(Received 16 April 2008; accepted 6 May 2008; published online 18 June 2008)

Current-voltage characteristics of $\text{Ga}_{0.99}\text{In}_{0.01}\text{As}$ tunnel diodes are studied experimentally and theoretically. Three possible tunneling mechanisms are considered: direct band-to-band tunneling, phonon-assisted tunneling through defects, and resonant tunneling through defects. Comparison between theoretical results and experimental data reveals resonant tunneling through oxygen-related defects as the dominant transport mechanism at voltages corresponding to the peak current in diodes with doping level about 10^{19} cm^{-3} . © 2008 American Institute of Physics.

[DOI: 10.1063/1.2936932]

Interband tunnel diodes are used to electrically interconnect the individual subcells in a metamorphic multijunction solar cell.¹ Since photons are only converted efficiently within the subcells, the tunnel diodes have to feature high optical transmissivity. Especially when used in a concentrator solar cell, the tunnel diodes also have to operate at very high current densities and low voltages. Hence, tunnel diodes represent one of the most critical elements of multijunction solar cells.

An AIXTRON multiwafer metal organic vapor phase epitaxy reactor (AIX2600 G3) with $8 \times 4 \text{ in}^2$ configuration was used to grow the tunnel diode structures on Ge substrates. The n - and p -GaAs layers were highly doped with Te ($N_d = 1 \times 10^{19} \text{ cm}^{-3}$) and C ($N_a = 3 \times 10^{19} \text{ cm}^{-3}$), respectively. About 1% of In was added to the GaAs in order to achieve lattice match to Ge. Ellipsometric characterization confirmed the optical parameters to correspond well to those of GaAs in the literature.² In the following, these $\text{Ga}_{0.99}\text{In}_{0.01}\text{As}$ layers will be referred to as GaAs. The tunnel diode devices have been processed by common wet-chemical processing. They were etched to mesa structures with 0.7 mm diameter and plated with metal contacts on top and bottom. Current-voltage (I - V) characterization presented in Fig. 1 (closed circles) was performed via a four-wire measurement technique.

The tunneling current can be conditioned by several possible tunneling mechanisms,^{3–13} namely, (i) direct band-to-band tunneling, (ii) phonon-assisted tunneling through defects, and (iii) resonant tunneling through defects. For different applied voltages different tunneling mechanisms can be dominant. Of highest importance is the tunneling mechanism responsible for the high peak current at low applied voltages. In order to reveal this mechanism, one should calculate the current at low applied voltages on the basis of different tunneling mechanisms and compare the obtained results. We performed these calculations for tunnel diode structures studied experimentally as described above. The parameters of the junction used in our calculations are col-

lected in Table I. We consider the tunnel diode as an abrupt junction of degenerate n -type and p -type semiconductors with quasi-Fermi levels F_n and F_p . In this approximation, the profiles of the conduction and valence band edges $E_c(x)$ and $E_v(x)$ across the depletion layer of the junction with the thickness $d = d_n + d_p$ (d_n and d_p are the thicknesses of the depletion layers in n -type and p -type semiconductors, respectively) can be obtained by simple analytical expressions (for example, see Ref. 14). The corresponding energy diagram in the case of thermal equilibrium is shown in Fig. 2. Note that all energies are measured from the bottom of the conduction band in the bulk of the n -type semiconductor $E_{c,0}^{(n)}$ and all coordinates are measured from the starting point of the depletion layer in the n -type semiconductor.

The current density j_{bb} through this junction provided by the direct band-to-band tunneling, i.e., by tunneling of electrons with energy E from the conduction band of the n -type semiconductor into the valence band of the p -type semiconductor can be calculated according to Ref. 15

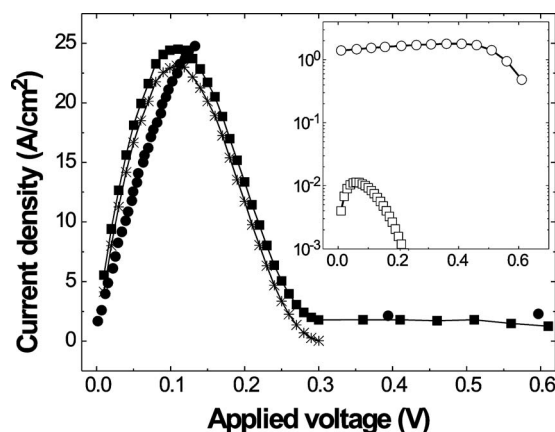


FIG. 1. Experimental I - V data (solid circles) along with theoretical results for the resonant tunneling (stars) and for the joint effects of resonant and nonresonant tunneling (solid squares) through defects ($N_d = 5 \times 10^{14} \text{ cm}^{-3}$). The insert shows the I - V curves calculated for the direct band-to-band tunneling (open squares) and for the nonresonant tunneling through defects (open circles).

^{a)}Electronic mail: kakhber.jandieri@physik.uni-marburg.de. Tel.: +49(0) 6421 2824159. FAX: +49(0) 6421 2827076.

TABLE I. Parameters of *n*-GaAs/*p*-GaAs homojunction in thermal equilibrium.

Parameter	Value
N_d	10^{19} cm^{-3}
N_a	$3 \times 10^{19} \text{ cm}^{-3}$
E_g^a	1.43 eV
ϵ^a	12.9
m_n^a	$0.063m_e$
m_p^{ha}	$0.051m_e$
m_p^{la}	$0.082m_e$
d	175 Å
d_n	135 Å
d_p	40 Å
$F_n=F_p$	0.232 eV

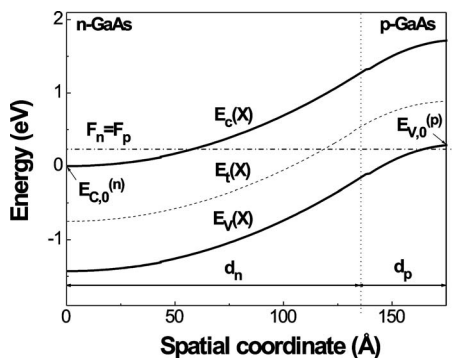
^aReference 2.

$$j_{bb} = \frac{e}{2\pi\hbar} \int_0^{E_{v,0}^{(p)}} [n_{2D}(F_n - E) - n_{2D}(F_p - E)] T_D(E) dE, \quad (1)$$

where

$$n_{2D}(E) = (mk_0T/\pi\hbar^2) \ln(1 + e^{E/k_0T}) \quad (2)$$

represents the density of electrons in a two-dimensional electron gas, m is the effective mass, k_0 is the Boltzmann constant, T is the lattice temperature, and $E_{v,0}^{(p)}$ is the valence band edge in the bulk of the *p*-type semiconductor. The transmission coefficient T_D through the potential barrier can be calculated either using the Wentzel–Kramers–Brillouin approximation,¹⁶ or the global transfer matrix technique.^{17,18} We use the latter approach. This method requires to approximate the actual potential profile by a set of narrow regions of constant potential in a stepwise manner. Then, the total transfer matrix and the total transmission coefficient through the arbitrary shaped potential barrier can be calculated by sequential multiplication of partial transfer matrices, each characterizing the transfer of an electron through the individual rectangular potential barrier. The results of our calculations in the case of direct band-to-band tunneling are presented in Fig. 1 (open squares in the insert). One can see that the calculated current is too low to explain the experimental data. Therefore, direct band-to-band tunneling cannot account for the high peak current and tunneling through defects should be considered.

FIG. 2. Energy diagram of *n*-GaAs/*p*-GaAs homojunction in the thermal equilibrium.

The tunneling through defects can occur via two different processes: phonon-assisted tunneling^{3–10} and resonant tunneling.^{5,11–13} The current j_t provided by the phonon-assisted tunneling can be considered as a tunnel-assisted recombination on the trap state E_t associated with the defect in the depletion layer of the junction.^{9,10} Instead of thermal emission over the entire trap depth, which is the only escape mechanism possible in the absence of the electric field in the junction, in real *p*-*n* junctions carriers can also be emitted by thermal excitation over only a fraction of the trap depth, followed by tunneling through the remaining potential barrier. It is also true for the recombination process on the trap. Consequently, j_t can be calculated according to

$$j_t = e \int_0^d R_t(x) dx, \quad (3)$$

where the tunneling-assisted recombination coefficient R_t can be calculated by the modified Shockley–Read–Hall formula,^{9,10} where instead of conventional lifetimes of the electrons τ_n and holes τ_p , the effective lifetimes $\tau_n^{\text{eff}} = \tau_n / (1 + \Gamma_n)$ and $\tau_p^{\text{eff}} = \tau_p / (1 + \Gamma_p)$ are used. These effective lifetimes are reduced due to tunneling effects by the factors^{9,10}

$$\Gamma_n = (k_0T)^{-1} \int_0^{\Delta E_n} e^{E/k_0T} T_D(E) dE, \quad (4a)$$

$$\Gamma_p = (k_0T)^{-1} \int_0^{\Delta E_p} e^{E/k_0T} T_D(E) dE, \quad (4b)$$

where for a given spatial location of the trap $E_t(x)$, the integration limit ΔE_n is determined by the difference between the local edge $E_c(x)$ of the conduction band, and either $E_t(x)$ or $E_{c,0}^{(n)}$ depending on which of them is closer to $E_c(x)$. The same can be said for ΔE_p , considering $E_v(x)$ instead of $E_c(x)$ and $E_{v,0}^{(p)}$ instead of $E_{c,0}^{(n)}$.

In order to calculate the defect-assisted tunnel current, one has to know the energy level of the defect centers and the recombination lifetimes of electrons and holes, controlled by these centers. We assume that the major defects in our structures are similar to the oxygen-related defects with energy level $E_t = -0.75$ eV Ref. 19 homogeneously distributed in the depletion layer of the *n*-GaAs/*p*-GaAs junction with concentrations below $N_t \sim 10^{15} \text{ cm}^{-3}$. The recombination lifetimes were determined according to their relation to the corresponding recombination coefficients β_n and β_p : $\tau_n = (N_t \beta_n)^{-1}$, $\tau_p = (N_t \beta_p)^{-1}$. The value $\beta_n \approx 7 \times 10^{-9} \text{ cm}^3 \text{ s}^{-1}$ is known.¹⁹ The value β_p for oxygen-related centers in GaAs is, however, not known precisely. Our calculations show that the variation of β_p in the range from $\beta_p \approx 5 \times 10^{-10}$ to $5 \times 10^{-9} \text{ cm}^3 \text{ s}^{-1}$ does not change the current-voltage characteristics essentially and that current in the case of light holes is significantly higher than that for heavy holes. Light holes contribute more than heavy holes to the tunnel-assisted currents due to their larger effective radius. Since the effective mass of the light holes $m_p^l = 0.082m_e$ differs only slightly from that of electrons $m_n \approx 0.063m_e$, and since the oxygen-related energy level in GaAs is situated nearly in the middle of the energy gap, the values of β_p chosen close to β_n seem to be reasonable. The results of our calculations are sensitive to the choice of the defect concentration. By taking different values of N_t and comparing the obtained theoretical results with the experimental data, one can conclude that the values

of the observed peak current could be achieved in the regime of nonresonant tunneling assuming the concentration of defects as high as $N_t \approx 8 \times 10^{15} \text{ cm}^{-3}$. This concentration seems unreasonably large. Moreover, even in such a case, the voltage corresponding to the maximum of the current would be much higher than the one observed experimentally and shown in Fig. 1. Furthermore, at such high defect concentrations the resonant tunneling process considered below would give much larger currents than those obtained by the expression (3). The insert of Fig. 1 shows the I - V dependence (open circles) obtained in the case of nonresonant tunneling through defects with $\beta_p = 2 \times 10^{-9} \text{ cm}^3 \text{ s}^{-1}$ and $N_t = 5 \times 10^{14} \text{ cm}^{-3}$. Although the values of the current density obtained on the basis of the defect-assisted nonelastic tunneling are much higher than those in the case of direct band-to-band tunneling (open squares), they are still much lower than the experimentally obtained values (solid circles). On the other hand, as it will become clear from below, for $N_t = 5 \times 10^{14} \text{ cm}^{-3}$ the resonant tunneling through oxygen-related defects would give a good agreement between the theoretical results and the experimental data. Therefore, one can exclude nonresonant currents as dominant process in the range of voltages corresponding to the peak current.

Let us now turn to the resonant tunneling through defects. We use the model proposed in Ref. 13. According to this model, a defect in a tunnel junction can be represented by a square potential well dividing the whole potential barrier into two potential barriers. Then, the resonant tunneling through defects can be considered as a double barrier problem. The electron transmission coefficient T_{tot} for one type of defects with the concentration N_t and the capture cross section σ is given by¹³

$$T_{\text{tot}} = \sigma N_t^{2/3} T_{\text{res}}, \quad (5)$$

where the resonant transmission coefficient T_{res} is given by

$$T_{\text{res}} = T_1 T_2 (1 + R_1 R_2 - 2\sqrt{R_1 R_2} \cos \Phi)^{-1}. \quad (6)$$

T_1 and T_2 are the transmission coefficients through potential barriers surrounding the potential well (representing the defect) at the left and right sides, respectively, $R_1 = 1 - T_1$ and $R_2 = 1 - T_2$ are the corresponding reflection coefficients from the barriers and $\Phi = 2kd_w + \theta_1 + \theta_2$ is the phase angle determined by the electron wave number k in the well, d_w is the width of the well, and θ_1 and θ_2 are the phase changes during the reflection from the left and the right walls of the well, respectively. The corresponding current density can be calculated according to Eq. (1) although using T_{tot} from Eq. (5) instead of T_D . The resonance takes place at energy E_{res} that satisfies the condition $\Phi = 2\pi n$ with integer n . The transmission rises dramatically near the resonance and it reaches its maximum value of unity if the structure is symmetric in the sense that $T_1 = T_2$, when there is perfect total transmission through the double barrier whatever opaque the individual barriers can be. In the case of a uniform distribution of defects in the junction, the condition of maximum resonant current depends on the applied voltage V_{app} and on the energy level of the defect E_t . Besides, according to Eqs. (5) and

(6), other important parameters for calculation of the resonant tunneling current are the capture cross section σ and the defect concentration N_t . The cross-section can be determined according to $\sigma = \beta_n (\bar{v}_T)^{-1}$, where \bar{v}_T is the thermal velocity of an isolated electron. For defects with $E_t = -0.75 \text{ eV}$ at $T = 300 \text{ K}$ we have $\sigma \approx 7 \times 10^{-16} \text{ cm}^2$ which is in good agreement with experimental data.¹⁹ Our calculations show that the resonant tunneling is able to account for the observed peak current at the appropriate applied voltage, provided the value of N_t is about $5 \times 10^{14} \text{ cm}^{-3}$. This value is considerably less than the oxygen detection limit of $\sim 10^{15} \text{ cm}^{-3}$ in the secondary-ion-mass spectroscopy measurements performed. The corresponding I - V dependences in the case of the resonant tunneling through defects (stars) as well as in the case of joint consideration of resonant and nonresonant tunneling (solid squares) are shown in Fig. 1. By comparing these results to experimental data (solid circles), we come to the conclusion that the resonant tunneling is the dominant transport mechanism at voltages corresponding to the peak current. Furthermore, a comparison between experimental data and the theoretical calculations reveals the concentration of defects N_t in the sample under study.

Financial support of the Fonds der Chemischen Industrie, of the Deutsche Forschungsgemeinschaft and of the European Graduate Program "Electron-electron interactions in solids" is gratefully acknowledged. This work was supported in part by the European Commission through the funding of the project FULLSPECTRUM (SES6-CT-2003-502620). The work of W. Guter is supported by the Deutsche Bundestiftung Umwelt.

¹T. Takamoto, E. Ikeda, H. Kurita, and M. Ohmori, *Appl. Phys. Lett.* **70**, 381 (1997).

²M. E. Levinstein and S. L. Romyantsev, *Handbook Series on Semiconductor Parameters* (World Scientific, London, 1996), Vol. 1.

³A. Schenk, *J. Appl. Phys.* **71**, 3339 (1991).

⁴A. Schenk, *Solid-State Electron.* **36**, 19 (1993).

⁵M. Herman and A. Schenk, *J. Appl. Phys.* **77**, 4522 (1995).

⁶M. Stadele, B. Fischer, B. R. Tuttle, and K. Hess, *Superlattices Microstruct.* **28**, 517 (2000).

⁷M. Stadele, B. R. Tuttle, and K. Hess, *J. Appl. Phys.* **89**, 348 (2001).

⁸M. Stadele, B. Fischer, B. R. Tuttle, and K. Hess, *Solid-State Electron.* **46**, 1027 (2002).

⁹G. A. M. Hurkx, D. B. M. Klaassen, and M. P. G. Knuvers, *IEEE Trans. Electron Devices* **39**, 331 (1992).

¹⁰G. A. M. Hurkx, H. C. de Graaff, W. J. Kloosterman, and M. P. G. Knuvers, *IEEE Trans. Electron Devices* **39**, 2090 (1992).

¹¹J. W. Gadzuk, *J. Appl. Phys.* **41**, 286 (1969).

¹²B. Ricco, M. Y. Azbel, and M. H. Brodsky, *Phys. Rev. Lett.* **51**, 1795 (1983).

¹³C. W. Jiang, M. A. Green, E. C. Cho, and G. Conibeer, *J. Appl. Phys.* **96**, 5006 (2004).

¹⁴N. W. Ashcroft and N. D. Mermin, *Solid State Physics* (Holt, Rinehart & Winston, New York, 1976), p. 596.

¹⁵L. Esaki, *Phys. Rev.* **109**, 603 (1958).

¹⁶L. D. Landau and E. M. Lifshitz, in *Quantum Mechanics* (Pergamon, Oxford, 1962).

¹⁷R. Redhammer and F. Urban, *Phys. Status Solidi B* **182**, 133 (1994).

¹⁸J. Racko, A. Grmanova, J. Parizek, and J. Breza, *Czech. J. Phys.* **47**, 649 (1997).

¹⁹D. V. Lang and C. H. Henry, *Phys. Rev. Lett.* **35**, 1525 (1975).